JOURNAL OF AIRCRAFT
Vol. 29, No. 6, Nov.–Dec. 1992

Heat Transfer Peculiarities in Supersonic Flows

V. Ya. Borovoy,* V. N. Brazhko,† G. I. Maikapar,‡ A. S. Skuratov,† and I. V. Struminskaya§
Central Aerohydrodynamic Institute (TsAGI), Moscow, Russia

A method of heat transfer and gas flow investigation based on the application of thermal sensitive coatings or thermocouple sensors and various visualization techniques is described. The thermal sensitive coatings and visualization reveal heat transfer peculiarities, and the complex nature of the method contributes to understanding the processes and generalization of quantitative results. Data concerning heat transfer on the leeward side of a blunt cone in the regions of the shock-wave boundary layer and bow wave interaction, in gaps and cavities of the orbiter's thermal insulation, and in the vicinity of them, are presented.

Nomenclature

a = tile length; plate semispan
b = thickness of high-pressure jet induced by shock interference
Ch = Stanton number
d = cylinder diameter
H = tile thickness
h = heat transfer coefficient
h_0 = heat transfer coefficient at sphere critical point
$\bar{h}$ = h/h_r
L = model length; distance from model leading edge to shock incidence point or gap beginning
l = gap length
M = Mach number
P_0 = total pressure
q = heat flux density
q_0 = heat flux at sphere critical point or critical line of cylinder
$R_{\infty,L}$ = $\rho_\infty U_\infty L/\mu_\infty$, Reynolds number
$R_{\infty,r}$ = $\rho_\infty u_\infty r/\mu_\infty$, Reynolds number
r = sphere or cylinder radius
S = surface distance
T = temperature
T_0 = stagnation temperature
u = velocity
w = gap width
x = longitudinal coordinate
y = transverse coordinate
z = normal-to-surface coordinate
α = angle of attack
Δ = tile protrusion (recession)
δ = boundary-layer thickness
δ^* = boundary-layer displacement thickness
θ = cone, wedge semiangle
λ = wavelength
μ = dynamic viscosity coefficient
ρ = density
φ = circumferential angle measured from windward line
χ = sweep angle

Subscripts
∞ = freestream conditions
e = boundary-layer edge conditions
m = maximum value
r = reference value
w = wall conditions
χ = critical cylinder line conditions at swept angle χ

Introduction

AMONG the most important features of vehicle aerodynamic heating are narrow regions on its surface where the heat flux density exceeds the density of the heat flux to the ambient surface several times (sometimes by an order of magnitude). The reasons for these peaks of the heat flux are complex gasdynamics phenomena: interaction of shock waves with each other and with the boundary layer, flow separation and attachment, vortices, and laminar-turbulent transition in the boundary layer and in mixing layers. Of interest also is a periodic variation of the heat flux value in the direction perpendicular to the gas flow that is associated with longitudinal vortices generated near the surface that are observed even in nominally two-dimensional flows, in particular, in case of a flow separation.

The conditions for the existence of the foregoing features (Mach and Reynolds numbers, angles of attack, and geometric characteristics) have not been investigated sufficiently. In calculations, considerable success has been achieved for only comparatively simple flow models, such as for plane shock wave impingement on a cylinder (two-dimensional flow). However, numerical calculation using the Navier-Stokes equations requires considerable machine time of the highest capacity computers. Even so, the required spatial resolution often is not achieved and, in the case of a turbulent flow, the result depends on the turbulence model used. Therefore, experimental methods will still retain their value as a source of information about complex three-dimensional flows and as verification of calculation methods over the long period.

At TsAGI (Central Aerohydrodynamic Institute), a complex method is used for the investigation of aerodynamic heating of vehicles and their components, which provides not only quanatitative results but also general concepts of gas flows.

Methods of Aerodynamic Heating Investigation

In various wind tunnels (long-duration and impulse wind tunnels), the well-known economical and efficient method of thermal sensitive coatings to obtain the continuous distribution of heat flux on the model surface is used widely. Thermal sensitive coatings with melting temperatures from 41 to 400°C[1] are used. The temperature measurement error is from 0.5 to 1°C. Model photography with time recording is used during the experiment. A digital image analysis sometimes is per-

Received June 2, 1991; revision received Oct. 5, 1991; accepted for publication Oct. 15, 1991. Copyright © 1991 by the American Institute of Aeronautics and Astronautics, Inc. All rights reserved.

*Head, Heat Protection Branch, Aerothermodynamic Division, 140160 Zhukovsky-3.
†Senior Scientist, Heat Transfer Branch, Aerothermodynamic Division, 140160 Zhukovsky-3.
‡Professor, Head, Aerothermodynamic Division.
§Leading Engineer, Heat Protection Branch, Aerothermodynamic Division, 140160 Zhukovsky-3.

formed in the course of data reduction. In order to obtain quantitative data, a model of one-dimensional heat propagation in a semi-infinite space is used most often, and the greatest errors in determining the heat transfer coefficient are associated with the fact that this model is incompatible with the experiment conditions. In the case of unknown boundary-layer conditions and nonisothermal surface, it is necessary to measure temperature as a function of time, and the known solution for the semispace can be used for processing. For introducing the corrections accounting for the heat conduction influence on heat flux peaks, it is possible to use the solution for the given distribution of the heat flux over the surface.[2] Inaccurate information about thermophysical characteristics of the materials used for model manufacturing is an additional source of errors. The accuracy of thermal sensitive coatings for a nonseparated flow is only somewhat less than the accuracy of measurements using discrete sensors. For separated flow regions, there appears another source of errors; namely, the recovery temperature uncertainty. It is not known whether there is a linear dependence of a heat flux on a temperature difference. This problem has not been studied sufficiently.

If it is impossible to film a model part, then a series of experiments of different duration is carried out. After each of such experiments, the model is disassembled and photographed.

Thermal sensitive coatings are also used in impulse wind tunnels with run times from 0.01 to 0.1 s. The thickness of the thermal sensitive coating should be very small in this case.

Characteristic examples of the application of thermal-sensitive coatings in long duration wind tunnels are given; namely, a complex-shaped model (Fig. 1), heat flux peaks beneath the vortices initiating on the fore part of the leeside of the wing with sharp, variable-sweep edges,[3] and heat flux peaks on a delta wing with cylindrical edges caused by entropy "vortices" coming from the blunt tip.[4] A heat flux peak appears also on the side surface of the external angle, imitiating an inlet due to the separated flow reattachment.[5] The thermal-sensitive coatings are very efficient in investigations of *microphenomena*, for example, laminar-turbulent transition behind a protruding roughness[6] and heat transfer in small cavities.[7]

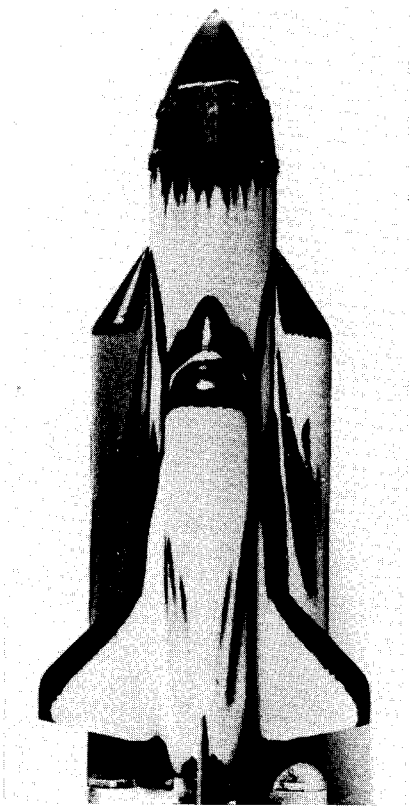

Fig. 1 "Energia-Buran," $M_\infty = 5$, $R_{\infty,L} = 3 \cdot 10^6$, $\alpha = 0$.

In some cases, when the application of thermal sensitive coatings is complicated because filming is impossible, surface foil thermocouples[8] 0.03-mm thick and 0.2-mm wide are applied in long-duration wind tunnels. They are bonded flush with the surface of the model, which is manufactured of a thermal isolation material. The data reduction is the same as in case of thermal sensitive coatings.

In impulse wind tunnels the "thin wall" method is applied. The thin wall is a 0.1–0.2-mm-thick foil that serves as a common thermoelectrode for a group of thermocouples. Thermoelectrode wires rolled a thickness of 0.5 mm are welded to the internal wall surface. The junction dimension is 0.2 × 0.2 mm.

In long-duration and impulse wind tunnels calorimetric heat flux sensors of 1–2-mm diam are used, their thickness being chosen depending on the experiment duration. The sensitivity of each sensor is measured by using a jet calibration setup.[9]

The second component of the complex method is gas flow visualization. Streamlines are obtained as a result of the flow of calibrated oil points, which are applied to the model surface by means of a special device.[10] They are very useful for representing the topology of the wall flow and, in particular, they reveal attachment lines often associated with heat flux peaks.

To obtain information on the flow structure throughout the whole disturbed flowfield, optical methods are used. The most simple of the known methods of the three-dimensional gas-flow visualization is the method of the "laser knife,"[1] which is a development of the vapor screen method. In one of the TsAGI wind tunnels, the particles required for this method are contained in kerosene combustion products in the air heater, so that no seeding of the air by light scattering particles is required. Characteristic structures (shock waves, expansion waves, vortices and separation regions) and small peculiarities, for example, longitudinal periodic vortices, are seen in the black-and-white pictures. An interesting example is flow about a delta wing in roll.[11] In front of one edge, the normal velocity component is less than the sound velocity; a subsonic vortex forms here. In front of the other edge, the normal component is greater than the sound velocity; a separation zone adjacent to the surface forms here.

In the base region of a twin-finned aircraft, the laser knife discovers bow and expansion waves from leading and side edges of the wing and horizontal tail, embedded shock waves, tip vortices with cone shocks surrounding them, and shocks from trailing edges.[3] The method can be improved; for example, the spectrum of limiting streamlines can be combined with the measurement of the heat flux using a thermal sensitive coating (Fig. 2) or with flow visualization using the laser knife (Fig. 3). Digital analysis of black-and-white pictures using reference colors for the lines of the same density of film makes it possible to obtain higher contrast flow pictures and reveal additional flow details.

Heat Transfer Peculiarities on Leeward Surface of a Blunt Cone

The heat transfer to blunt cones $\theta = 5$–15 deg with the angles of attack $\alpha = 0$–55 deg was investigated by the method

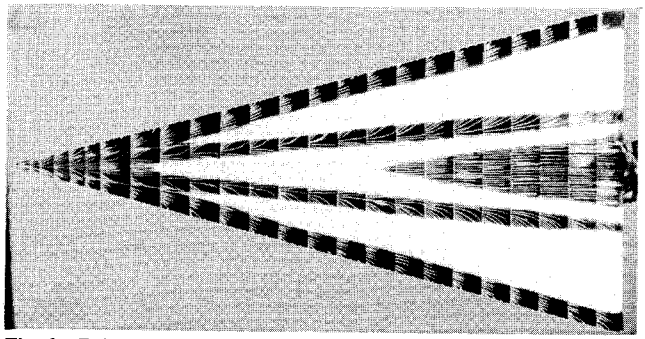

Fig. 2 Delta Wing. $M_\infty = 4$, $R_{\infty,L} = 3 \cdot 10^6$, $\chi = 75$ deg, $\alpha = 5$ deg.

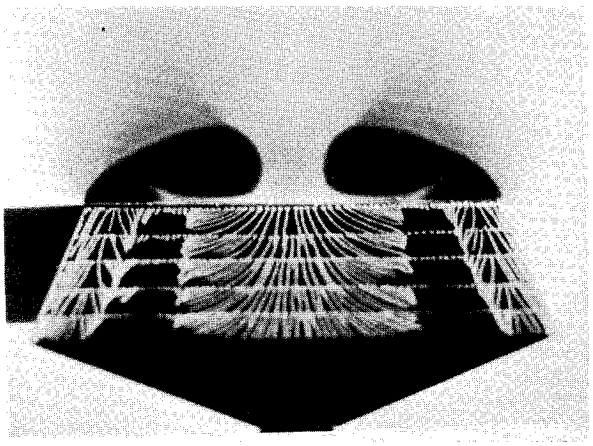

Fig. 3 Delta Wing. $M_\infty = 3$, $R_{\infty,L} = 4 \cdot 10^6$, $\chi = 75$ deg, $\alpha = 15$ deg.

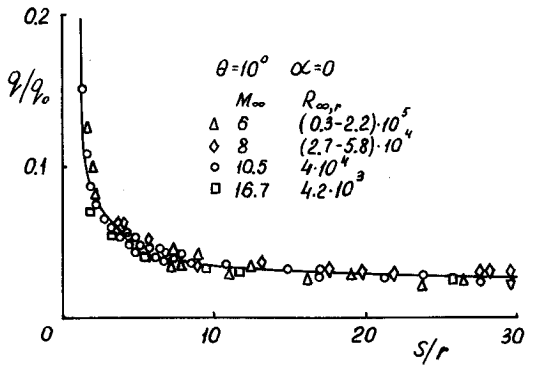

Fig. 4 Heat transfer distribution, blunt cone.

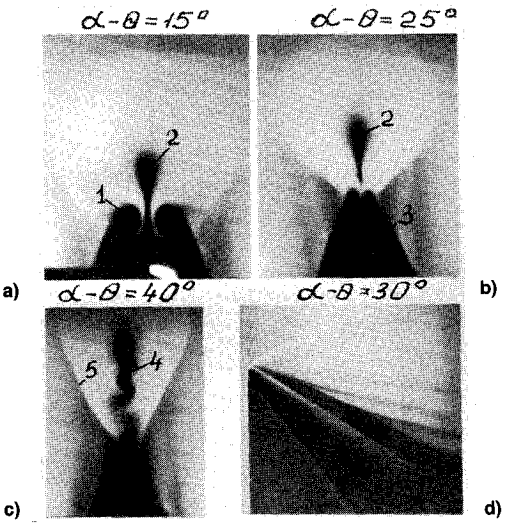

Fig. 5 Blunt cone, laser knife, $M_\infty = 3$, $R_{\infty,L} = 3 \cdot 10^6$, $\theta = 10$ deg: 1) vortices, 2) entropy wake, 3) near-wake, 4) far wake, and 5) afterbody shock.

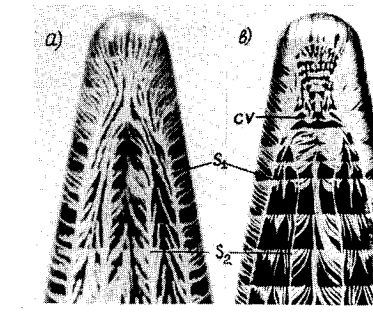

Fig. 6 Surface streamlines, $\theta = 10$ deg, $\alpha = 30$ deg: a) $M_\infty = 5$, $R_{\infty,r} = 4.3 \cdot 10^4$, and b) $M_\infty = 3$, $Re_{\infty,r} = 1.3 \cdot 10^5$; S_1, primary separation; S_2, secondary separation; and CV, concentrated vortex.

of thermal sensitive coatings. The Mach number was $M_\infty = 3$–16.7, the Reynolds number was $R_{\infty,r} = 4.2 \cdot 10^3$–$2.8 \cdot 10^5$, and the temperature ratio was $T_w/T_0 = 0.17$–0.7.

In a hypersonic laminar flow, there is a stabilization of the distribution of the heat transfer density ratio q/q_0 (Fig. 4) (q_0 is the Fay and Riddell theory). The solid curve shows the calculated result without taking into account of the entropy effect.[12] As expected,[13,14] the entropy effect has a small influence on the laminar heat transfer.

The visualization of a flow about blunt cones using the laser knife has shown that at the same values of $\alpha-\theta$ a qualitative similarity of leeward separation flows is observed. The separation initiates at $\alpha-\theta \approx 0$. As the angle of attack increases, two narrow separation zones adjacent to the cone surface form and then turn into two vortices, separated from the surface (Fig. 5a). There is an entropy wake from the bluntness between vortices.

When the flow velocity component normal to the cone axis exceeds the sound velocity, the vortices transform into two closed separation regions (Fig. 5b) having rectilinear boundaries at great values of $\alpha-\theta$. This flow is similar to the near wake behind the cylinder that is in a supersonic transverse flow. The entropy wake emerges over separation regions and, with a further increase in $\alpha-\theta$, turns into a far wake (Fig. 5c). Discrete stationary vortices come out of the near wake periodically along the cone length (Fig. 5d). For the visualization of these vortices the laser knife plane was oriented parallel to the plane of the angle of attack.

The separation can be "open"[15] (Fig. 6a) or "closed" (Fig. 6b). For an open separation, the line of the initial separation S_1 in the fore cone part is not closed and the gas from the nose, not separating, moves into the leeside region lying between unclosed branches of the separation line. For a closed separation, the initial separation line S_1 in the fore cone part is closed, and the gas can come into the leeside zone only after separation from the cone surface. In the forward part of the separation zone, a return flow region forms in which the gas flows in the direction opposite to the freestream. A concentrated vortex CV follows after it.[16] Further aft there is the main separation zone with longitudinal vortices. Along with the initial separation, a secondary and successive separations take place in this zone. The variation of Mach and Reynolds numbers has great influence on the shape and position of the separation region and, consequently, also on the heat transfer to the leeside cone surface, which was noted in Reference 17. In particular, at an angle of attack $\alpha = 30$ deg an increase in the Mach number and a simultaneous decrease in the Reynolds number transformed closed separation into an open one (Fig. 6).

The influence of α on the heat transfer to the leeside cone generatrix ($\varphi = 180$ deg) is shown in Fig. 7a. At $\alpha = \theta$ an increased heat transfer region forms near the cone base section. As the angle of attack increases this region displaces forward, and the second peak of the heat flux forms.

At a constant angle of attack, a decrease in the apex semiangle θ has the same influence on the heat transfer as an increase in the angle of attack (Fig. 7b).

An increase in the Mach number has a different influence on the heat transfer in the region of a nonseparated and a separated flows (Fig. 8): in the region of nonseparated flow (at $S/r \lesssim 1$), the heat flux varies weakly; in the region of separated flow, the heat transfer decreases with an increase in the Mach number.

Figure 9 shows the heat transfer distribution over the cone cross section. As the Mach number increases, the heat flux in the attachment region decreases by an order of magnitude. At the same time, its distribution changes: at $M_\infty = 3$ two sharply pronounced peaks exist because of attachment region branching (Fig. 9a); at $M_\infty = 10.5$ only one heat flux maximum that is smeared (Fig. 9c) forms. The dash lines in Fig. 9b show

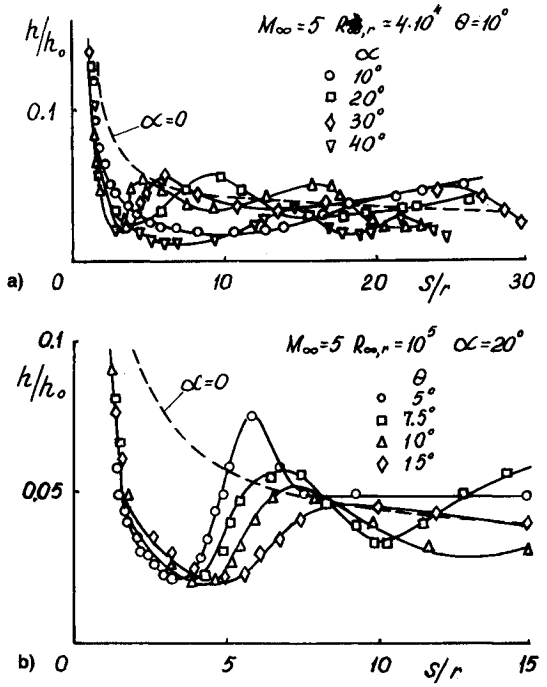

Fig. 7 Blunt cone, heat transfer distribution along its length.

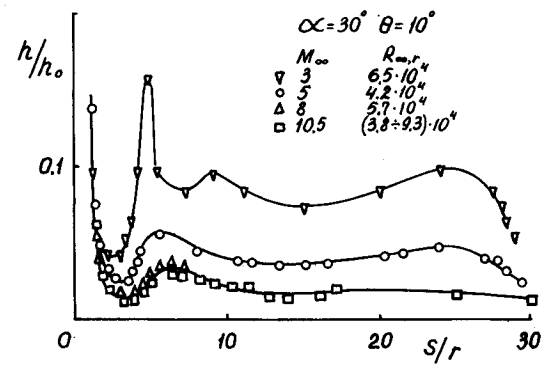

Fig. 8 Blunt cone, heat transfer distribution along its length.

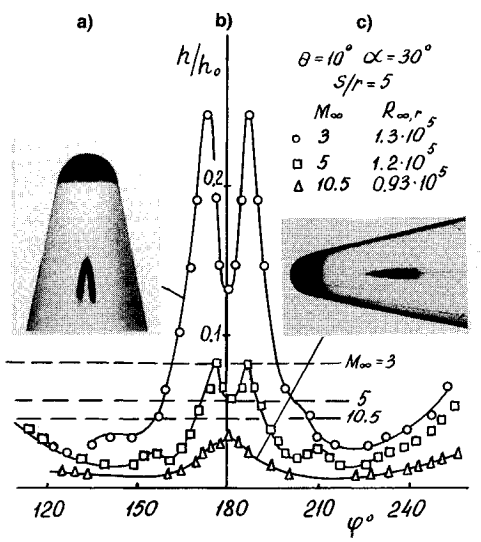

Fig. 9 Heat transfer distribution over cross section of blunt cone.

heat flux levels in the section considered at $\alpha = 0$. In a hypersonic velocity range ($M \gtrsim 10.5$) the values of h/h_0 throughout the whole leeside surface at $\alpha = 30$ deg are considerably less than at $\alpha = 0$.

Figure 10 summarizes results for h_m/h_0 in the attachment region on the leeside cone surface with $\theta = 10$ deg at $\alpha = 30$ deg and at different values of M_∞ and $R_{\infty,r}$.

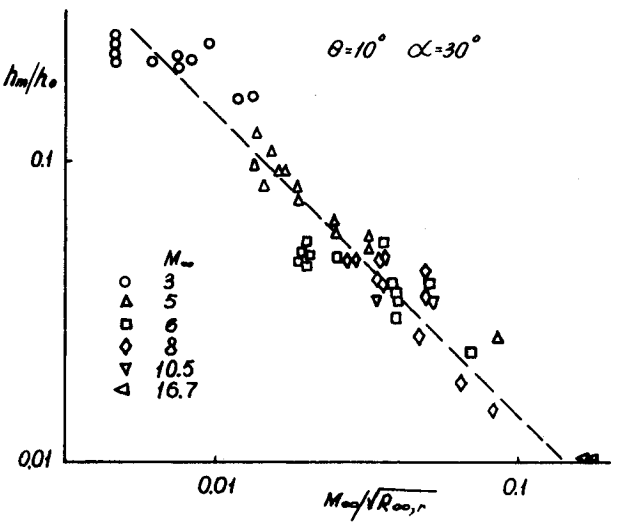

Fig. 10 Correlation of maximum heat flux values.

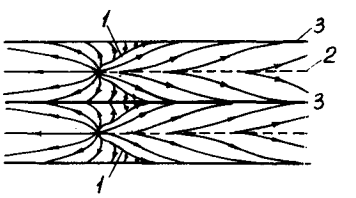

Fig. 11 Surface streamline pattern in reattachment region.

Periodicity of Transverse Heat Flux Distribution

In some flows, there is a periodic variation of flow parameters in the direction perpendicular to the mean velocity. It is usually associated with the formation of a system of longitudinal vortices of the Taylor-Goertler type. The transverse periodicity seems to have been detected for the first time in Ref. 18 when a laminar separation flow was investigated behind a forward facing step. The flow periodicity in the reattachment region becomes apparent most strongly in the heat transfer to the body surface.[19,20] In the reattachment region, a system of narrow zones of increased and decreased heat transfer forms, and the maximum heat transfer coeffient may exceed the minimum several times. Three-dimensional periodic flow singularities were also revealed in the reattachment region of a supersonic turbulent boundary layer behind an axisymmetric step[21,22] and a plane[23] step.

This article reports some results of the experimental investigations of the flow and heat transfer in the separation and reattachment regions of nominally two-dimensional supersonic flows behind a step, in front of a flap, and as a result of a shock wave impingement on the boundary layer. The tests were carried out in short- and long-duration wind tunnels at Mach numbers $M_\infty = 4$–12.8 and unit Reynolds number $(1–62)\cdot 10^6$ 1/m. The boundary layer in front of the separation was laminar in most cases. In a general case, the attachment line is formed by a set of arcs 1 (Fig. 11) placed periodically in the cross direction. The arcs are the divergence lines. Another divergence line 2 forms in each three-dimensional cell limited by the separation lines 3. The heat flux on the divergence lines 2 has a maximum, while on the separation lines 3 it is a minimum.

Such a picture is realized during the separation of a thin laminar boundary layer; in a thick boundary layer it is realized at a weak intensity of the disturbance that caused the separation. In case of high intensity, the attachment line degenerates into a straight line with node and saddle points on it.[18,22] The flow periodicity propagates from the attachment line forward inside the separation zone. This situation also occurs in the attachment of the turbulent boundary layer.[22] The transverse flow periodicity is also revealed on the boundary-layer

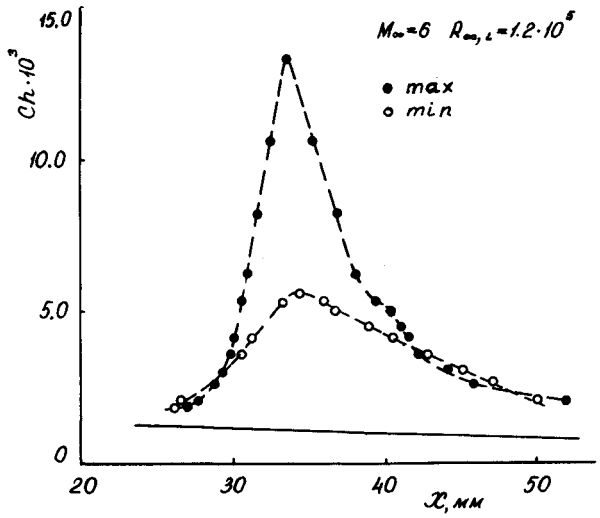

Fig. 12 Impingement of a shock from wedge θ = 15 deg on the plate, longitudinal heat flux distribution.

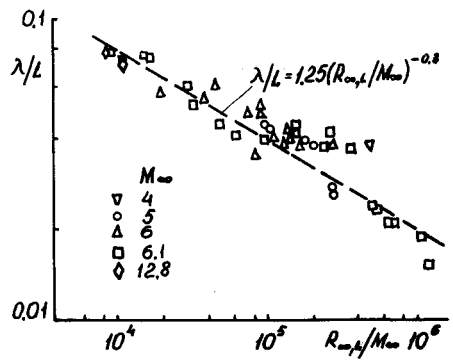

Fig. 13 Impingement of a shock from wedge θ = 15 deg on the plate, wavelength.

separation line. The wave length λ (distance between attachment lines) in the separation region is approximately equal to the wavelength in the attachment region.

The results for plate heat transfer in the separation zone caused by an incident shock wave from a wedge with an angle θ = 15 deg at M_∞ = 5 and $R_{\infty,L} = 10^6$ indicate how stationary and repeatable is the flow considered. Although the heat transfer coefficients changed somewhat in the repeated experiment, the position of the maximum and minimum lines remained invariable. In Ref. 22 it is shown that the cross-pressure distribution in the reattachment region also remained invariable in numerous repeated experiments that were carried out in a turbulent boundary layer.

Fig. 12 presents longitudinal distributions of the *Ch* for the section passing through a local maximum and for the section passing through a neighboring local heat transfer minimum. The solid line shows the calculated distribution of *Ch* in a freestream flow.

As the Reynolds number increases, the heat transfer coefficient ratio in the reattachment region rises, while the mean wave length λ decreases. The Mach number has an inverse influence on the wavelength. Figure 13 shows the dependence of the wave length ratio λ/L on the nondimensional parameter $R_{\infty,L}/M_\infty$ for the reattachment region of the flow separated from the plate surface under the action of a shock wave.

Periodic zones of increased heat transfer were also present in a number of other cases: in a nonseparated supersonic flow about cones with an isentropic compression surface,[24] on the leading edge of a variable sweep wing,[25] and in the reattachment region of the flow separated from the leeside of a delta semiwing mounted on the plate.[26] The maximum heat flux values in the attachment region in these cases, as well as in Fig. 12, exceed minimum values approximately by a factor of two.

Heat Transfer to Cylinder in Shock Wave Impingement Zone

One of the first papers devoted to this problem is Ref. 27. It was shown that, in case of a shock wave impinging on a cylinder that is perpendicular to the freestream flow, a high power jet forms that may cause a local pressure increase and intensify the heat transfer. In Ref. 28, the variation of the heat flux density was investigated in the impingement zone of the oblique shock wave as a function of the cylinder inclination angle. In Ref. 29, a phenomenological classification of the shock-wave interaction types was performed on the basis of the results of the flow and heat transfer in the impingement zone of the shock wave on a sphere. The predictions based on the experiments and approximate calculations[30] show that the heat transfer increases drastically as the Mach number rises. But, so far, the experimental investigations were carried out only up to M_∞ = 6. At higher Mach numbers, experiments of this kind were performed only in helium. This paper presents the results of a systematic experimental heat transfer investigation in the zone of the shock-wave interference with the laminar boundary layer in air flow at a high Mach number of M_∞ = 15.5. The experimental results are presented in more detail in Ref. 31.

A cylinder of r = 12.5-mm radius of a length 205 mm was equipped using the thin wall method with 60 heat flux sensors mounted along the attachment line. The minimum distance between the sensors in the shock-wave impingement zone was 1 mm. A wedge θ = 20 deg served as a shock generator. The shock inclination angle at the impingement on the cylinder was 27 deg.

The experiments were carried out in a shock tunnel at a total pressure $P_0 = 50 \cdot 10^5$ Pa, stagnation temperature T_0 = 1650 K, Reynolds number $R_{\infty,r} = 0.7 \cdot 10^4$. The run flow time was $7 \cdot 10^{-3}$ s.

The measurement results of a maximum heat flux are given in Fig. 14. The dashed lines show the calculation results for the heat flux ratio (use was made of the relations for the plane shock waves; it was assumed that the heat flux ratio is equal to the square root of the pressure ratio). The abscissa shows the interference types according to the classification of Ref. 29, which were determined using schlieren pictures. In case of II and V interference types, two pairs of heat transfer rate peaks form, which are shown in Fig. 14a by open and closed symbols. For these interference types, the calculation refers

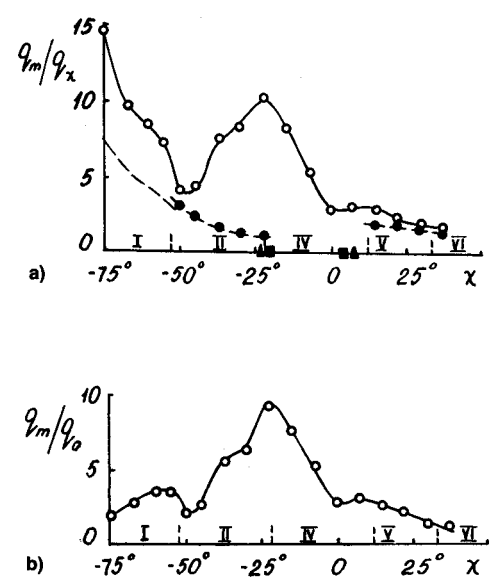

Fig. 14 Influence of cylinder slip angle on heat transfer (q_χ calculation for isolated sliping cylinder; q_0 calculation for isolated cylinder at χ = 0); ○ ●, experiment; ---, calculation; ▲, sonic line on cylinder; ■, sonic line on bow wave.

to smaller peaks. The ratio q_m/q_χ attains a maximum value at the *I* interference type (Fig. 14a). But the ratio q_m/q_0 (and, consequently, also the absolute heat transfer rate q_m) reaches a maximum value in case of the IV interference type (Fig. 14b). It takes place not at $\chi = 0$, as it might be expected, but at a considerable cylinder inclination ($\chi = -22$ deg).

The calculated curve in case of type I interference is similar to the experimental data. At the same time, the calculated values of q_m/q_χ are less than the experimental values by a factor of approximately two. This discrepancy is attributed to the fact that the shock waves impinging on and reflected from a cylinder cause a boundary-layer separation on the cylinder. The separation zone induces a shock wave, causing an additional pressure increase.

In case of type II interference (Fig. 15) a weaker shock wave O_2I_2 is reflected regularly from the cylinder surface, and the calculated heat flux ratios coincide essentially with experimental values (Fig. 14a). A stronger shock O_1I_1 cannot be reflected regularly from the cylinder surface. A terminating normal shock wave seems to form behind the shock O_1I_4, and the high-power gas jet that passed through the shock OO_1 and successive shocks spreads upward and downward along the cylinder generatrix, causing a considerable heat transfer increase. This flow is similar to the flow in type IV interference.

Type IV interference (Fig. 16) was observed in a sufficiently wide range of sweep angles: from $\chi = -22$ deg to $\chi = +7$ deg (type III interference was not identified). According to the calculation, the pressure behind a normal shock wave at point I_1, when $\chi = -22$ deg, exceeds 19.3 times the pressure

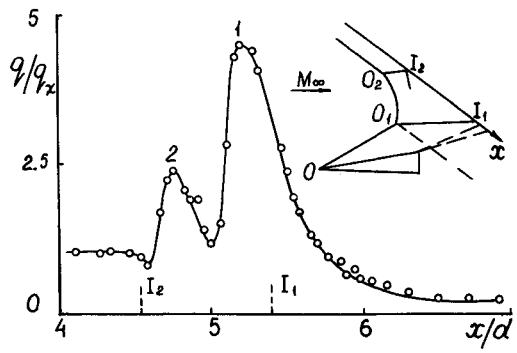

Fig. 15 Type II interference.

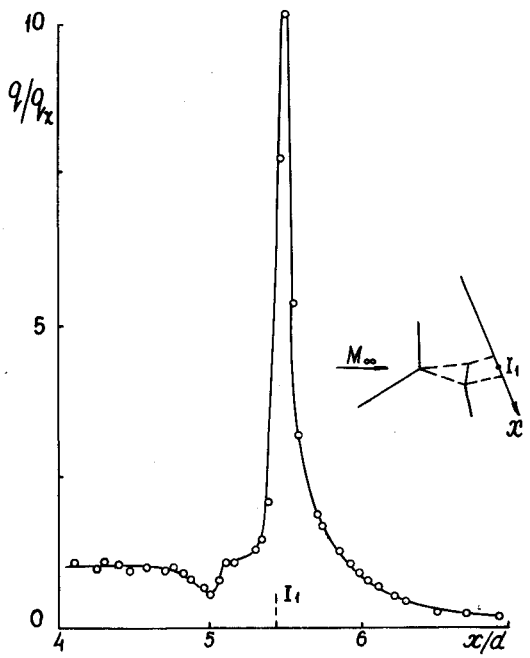

Fig. 16 Type IV interference.

on an isolated cylinder at the same sweep angle. To evaluate the maximum heat flux, it is necessary to know the jet thickness *b* also. Based on a shadowgraph picture, the following values were obtained: $b/d = 0.045$ at $\chi = -22$ deg, $b/d = 0.024$ at $\chi = -7$ deg. The calculated maximum heat flux values exceed tens of times the heat flux on an isolated sweeped cylinder, which differs greatly from the experimental values. It is not less important that, according to the adopted calculation procedure, the maximum heat flux rises as the angle χ increases because the jet becomes thinner, while in reality it decreases.

The most probable reason for a quantitative and qualitative discrepancy between calculated and experimental heat flux values in case of type IV interference is that a high-power jet mixing with a low-power gas is smeared, and at the cylinder surface, it has a decrease total pressure and an increased thickness. These effects become more pronounced because of a decrease of the local Reynolds number as the Mach number increases in the wind tunnel.

At sweep angles $\chi = 15$–30 deg, the flow in the interference zones refers to type V. This range of angle χ is in agreement with the calculated results presented in Ref. 32 for Mach number $M_\infty = 15$. Two zones of increased heat flux form on the cylinder surface. The calculated estimates of the heat flux for one of these zones considerably exceed the experimental values. For example, at $\chi = 22$ deg, according to the calculation, $q_m/q_\chi = 1.92$, and from the experiment $q_m/q_\chi = 1.26$. Similar discrepancies in the maximum pressure values are established in Ref. 32. The reason for this discrepancy is also revealed in that paper: it is assumed in the estimates that the impinging shock has a rectilinear shape behind the point of intersection with the bow cylinder shock wave; in reality it distorts under the action of the pressure difference and becomes weak.

Gas Flow and Heat Transfer in Elements of Orbiter Thermal Isolation

Gas flow and heat transfer in intersecting tile gaps were studied on a fragmentary model, mounted on a wind-tunnel wall, at $M_\infty = 6$. The displacement thickness of the turbulent boundary layer varied within the range of $\delta^* = 8.8$–12.2 mm. Total pressure and stagnation temperature fields were measured. The velocity profile in a turbulent boundary layer far away from a gap are approximated $u/u_\infty = (z/\delta)^{1/9}$. Near a gap edge the velocity profile is distorted, becoming truncated. A similar situation is known to occur in a turbulent boundary layer on a rough surface.[33] In this case, the heat transfer coefficient is greater than on a smooth surface.

Parameters governing heat transfer are found and the correlation formulas presented below for a heat transfer coefficient ratio $\bar{h} = h/h_r$ on different surfaces forming intersecting gaps (h_r is the measured heat transfer coefficient far away from a gap) are obtained.

1) On the external surface in the vicinity of a longitudinal gap

$$\bar{h} = 1 + \frac{0.31\, x/l}{(y/w)^{0.73}} (R_{\infty,L})^{0.084} \qquad (1)$$

The coordinate *x* is measured from the longitudinal gap beginning, coordinate *y* is measured from the edge of the gap, and *w* is the gap width. The formula is valid for $0.1 < x/l < 0.9$, $y \gtrsim 3r$ (*r* is the edge roundness radius). In the experiments, the gap length was $l = 0.15$ m, the length of the preceding surface section is $L = 1$ m.

2) On the internal longitudinal gap surface

$$\bar{h} = (0.25 + 0.90(x/L)^{1.22}) e^{-0.51 z/w} R_{\infty,L}^{0.084} \qquad (2)$$

3) In the gap intersection region (on the external surface)

$$\bar{h} = 1 + 2.5 \cdot 10^{-2} (l/x)^{1.21} (\delta^*/w)^{-0.52} \qquad (3)$$

The coordinate x is measured from the transverse gap edge, $x \gtrsim 3r$.

4) In the gap intersection region (on the internal surface)

$$\bar{h} = 3.80 - 1.10\,K^{0.62} \quad \text{at} \quad 0.04 < K < 2.50$$

$$\bar{h} = 3.80 - 1.77\,K^{0.18} \quad \text{at} \quad K > 3.5 \qquad (4)$$

where $K = (\delta^*/w)^2 z/l$, $z \gtrsim 3r$. The coordinate z is measured into the gap depth.

Another series of the investigations of aerodynamic heating in thermal isolation elements was carried out on geometrically similar models of the forebody of the orbiter (Fig. 17) of a scale 1:15. Longitudinal and transverse grooves were made on one model half. As a result of the intersection of these grooves, an orthogonal net has formed that imitates the orbiter's thermal isolation system. The dimensions of the tiles were 10 × 10 × 4 mm, which corresponds in this scale to the size of a full-scale tile. The width of the gaps between the tiles was 0.2 mm. The other model half was left smooth for purposes of comparison. One of the tiles in the forward part of the lower surface was made movable and it could be protruded or recessed. The investigations were carried out in large wind tunnels at $M_\infty = 7$; 12.7 and 13.7 and $Re_{\infty,L} = (1\text{–}12)\cdot 10^6$ (here L is the total orbiter length in a given scale).

Fig. 17a presents a photograph of a lower model surface. The melting of the thermal sensitive coating on the model afterbody indicates that the heat flux increases, it is caused by a boundary-layer transition. Fig. 17b gives a relative heat transfer coefficient distribution over a tiled (1) and a smooth (2) surface. The transition on the tiled surface begins earlier than on the smooth one, which is attributed to the destabilizing influence of intersecting gaps on the boundary layer.

The tile gaps lead also to a local increase in heat transfer. Figure 18 shows a dependence of the heat transfer coefficient ratio $\bar{h} = h/h_r$ at several points of the external surface on the tile installation height (h_r is the heat transfer coefficient in the center of a flush-mounted tile). The measurements were carried out using foil thermocouples. The boundary layer on the model surface was laminar. A tile protrusion $\Delta/a > 0$ results in a heat transfer increase at the point T. The heat transfer decreases on the surface following the protruding tile, and also in the vicinity of the longitudinal gap (point M). In

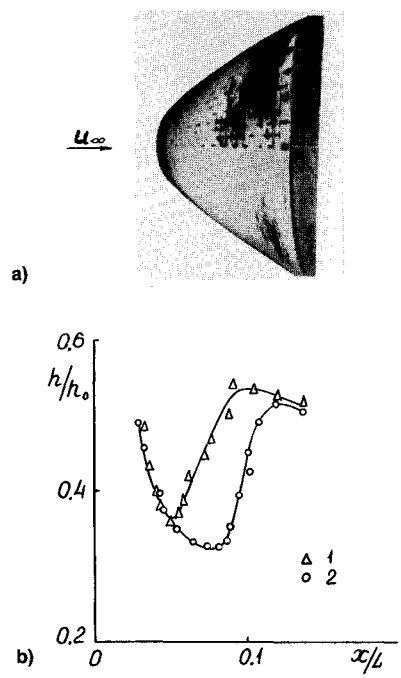

Fig. 17 "Buran" orbiter forebody model; $M_\infty = 7$, $R_{\infty,L} = 1.19\cdot 10^7$, $\alpha = 34$ deg.

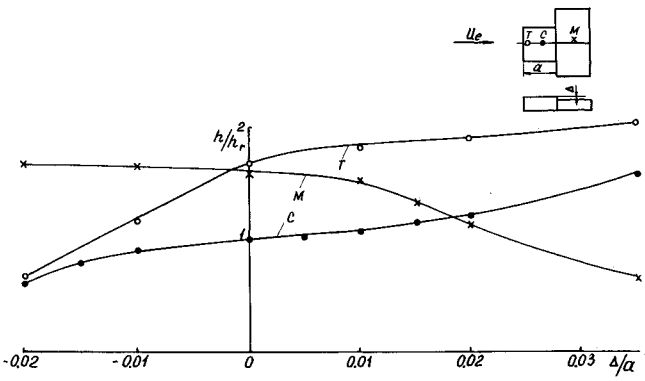

Fig. 18 Tile protrusion and recess influence on heat transfer, $M_\infty = 12.7$, $R_{\infty,L} = 10^6$, $\alpha = 34$ deg.

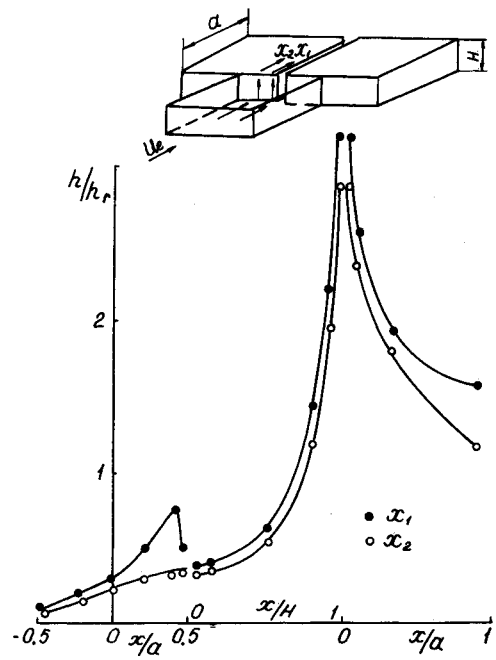

Fig. 19 Heat transfer in the fallen-out tile zone, $M_\infty = 13.7$, $R_{\infty,L} = 10^6$, $\alpha = 34$ deg.

case of a recessed tile $\Delta/a < 0$, the heat flux to its surface becomes less but it increases on the surface of the next tile.

Figure 19 presents a heat transfer coefficient distribution $\bar{h} = h/h_r$ on the cavity surface formed by a "fallen out" tile (h_r is the heat transfer coefficient at the center of the tile situated upstream of the cavity). Foil thermocouples were used. The distribution of $\bar{h}$ corresponds to the physical gas-flow pattern in the cavity.[34] The greatest increase in heat transfer takes place in the upper part of the back wall and on the external surface immediately behind the cavity. This is associated with the attachment of a viscous mixing layer to the surface and the great velocity and temperature gradients arising as a result of it.

The heat transfer in the lower part of the back wall and at the cavity bottom is controlled by a circulation flow. Because the boundary layer grows from the back wall to the forward wall in accordance with the flow direction at the cavity bottom, the value $\bar{h}$ drops in this direction. The cavity imitating a fallen-out tile has an exit into a longitudinal gap on the back wall, which considerably influences the heat transfer. The heat transfer coefficient near the gap on the back wall and behind the cavity is 10–20% greater than far away from it. It is associated with the action of the same mechanism that causes an increase of the heat transfer in a longitudinal flow near a gap. The gap also influences the heat transfer at the cavity bottom. The distribution of $\bar{h}$ over the bottom along the axes

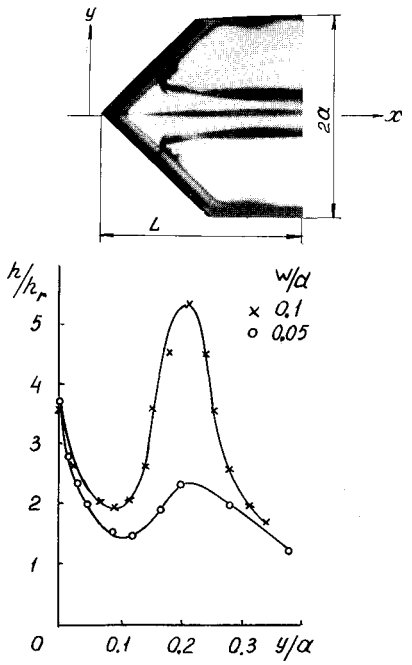

Fig. 20 Heat transfer on a wing with a groove on leading edge $M_\infty = 5$, $R_{\infty,L} = 1.07 \cdot 10^6$, $\chi = 45$ deg, $\alpha = 0$, $x/L = 0.75$.

x_1 and x_2 is essentially different. Near the back wall along the x_1-axes there is a maximum $\bar{h}$, whose occurrence is associated with the presence of the attachment line; a gas portion is involved into a return circulation flow, the other part flows into a gap behind the cavity. Far away from the gap, the heat transfer coefficient distribution over the bottom is monotone.

In order to examine the influence of technological joints and gaps on the gas flow and heat transfer at the leading edge of a wing, triangular plate models were used on whose cylindrical leading edges transverse grooves of square cross section were made. Some dark bands corresponding to increased heat transfer zones are seen in a picture of the model with a thermal sensitive coating (Fig. 20). The groove in this case can be considered to be a cavity in a flow directed along the leading edge. It is known that a vortex flow forms in such a cavity. The formation of a vortex in the groove was visualized by the schlieren method, and the distribution of the vortex above the wing with the aid of a laser knife.

An increase in heat transfer takes place on the wing symmetry line ($y/a = 0$) and under the vortices ($y/a = 0.2$) (see Fig. 20). The influence of the groove on heat transfer rises as its width w increases (Fig. 20), edge sweep angle decreases (in the range examined $\chi = 40$–75 deg) and the Reynolds number $R_{\infty,r}$ increases. A generalized parameter

$$(w/2r) \cos \chi \sqrt{R_{\infty,r}}$$

is introduced to define the influence of the values given above. The investigations were performed at $M_\infty = 5$ and 6 in the range of the aforementioned parameter variation from 1.8 to 47.0. At $\alpha = 0$, an increase in the heat transfer on the plate surface occurred only in the case of the parameter value greater than 11.

Conclusions

Heat transfer peaks and their periodic distribution occur rather often in supersonic three-dimensional gasflows near vehicles. These heat transfer peculiarities are caused by various factors, they depend considerably on similarity parameters; their variety complicates the possibility of their detection and study. An effective means of the experimental investigation is the heat flux measurement using thermal sensitive coatings and microcalorimeters and the visualization of a surface flow and flow as a whole by means of a laser knife. A systematic experiment often helps to do a correlation. The problem of scaling the results to hypersonic velocity flight conditions still remain unsolved.

References

[1]Borovoy, V. Ya., *Gas Flow and Heat Transfer in Zones of Shock Wave-Boundary Layer Interference* (in Russian), Mashinostroyeniye, Moscow, 1983, pp. 7–9, 20–25.

[2]Brazhko, V. N., Kovaleva, N. A., and Maikapar, G. I., "Heat Flux Measurement Method Using Thermal Sensitive Coatings" (in Russian), *Uchenye Zapiski TsAGI,* Vol. 20, No. 1, 1990, pp. 1–12.

[3]Maikapar, G. I., "Leeside Flow in a Supersonic Stream" (in Russian), *Sovremennye Problemy Aeromekhaniki,* Mashinostroyeniye, Moscow, 1987, pp. 103–113.

[4]Kondratyev, I. A., and Yushin, A. Ya., "On Appearance of Heat Transfer Peaks on the Windward Side of a Delta Wing with Blunt Leading Edges" (in Russian), *Uchenye Zapisky TsAGI,* Vol. 21, No. 1, 1991, pp. 89–92.

[5]Maikapar, G. I., and Pyatnova, A. I., "Flow at an External Corner of a Supersonic Aircraft Inlet Cowl" (in Russian), *Uchenye Zapiski TsAGI,* Vol. 11, No. 3, 1980, pp. 101–105.

[6]Skuratov, A. S., and Fedorov, A. V., "Experimental Investigation of Laminar-Turbulent Transition Behind a Three-Dimensional Roughness in a Boundary Layer on a Sharp Cone" (in Russian), *Izvestiya AN SSSR, Mekhanika Zhidkosti i Gaza,* No. 4, 1990, pp. 60–66.

[7]Borovoy, V. Ya., and Yakovleva, L. V., "Heat Transfer in Supersonic Flow about an Individual Round Cavity" (in Russian), *Izvestiya AN SSSR, Mekhanika Zhidkosti i Gaza,* No. 5, 1991, pp. 48–52.

[8]Borovoy, V. Ya., and Kolochinsky, Yu. Yu., "Surface Thermocouples as a Investigation Means of Heat Transfer on Models Tested in Intermittent Wind Tunnels" (in Russian), *Trudy TsAGI,* Issue 2340, 1987, pp. 148–155.

[9]Bogdanov, V. V., Kolochinsky, Yu. Yu., and Pleshakova, L. A., "Devices for Measuring Heat Transfer Rate in Short-Duration Wind Tunnels" (in Russian), *Trudy TsAGI,* Issue 1978, 1979, pp. 27–34.

[10]Brazhko, V. N., "Method of Visualization of Streamlines on Model Surface in Wind Tunnels," (in Russian), *Trudy TsAGI,* Issue 1749, 1976, pp. 241–256.

[11]Maikapar, G. I., "Separation Zones at the Leeside of a Delta Wing and a Body of Revolution in a Supersonic Flow" (in Russian), *Uchenye Zapisky TsAGI,* Vol. 13, No. 4, 1982, pp. 22–33.

[12]Bashkin, V. A., and Kolina, N. P., "Friction Drag and Heat Transfer Calculation on Spherically Blunted Circular Cones in a Supersonic Flow" (in Russian), *Trudy TsAGI,* Issue 1106, 1968, pp. 192–267.

[13]Murzinov, I. N., "Laminar Boundary Layer on Blunt Bodies with Accounting for the External Flow Vorticity" (in Russian), *Izvestiya AN SSSR, Mekhanika Zhidkosti i Gaza,* No. 6, 1966, pp. 124–129.

[14]Kolina, N. P., Pyatnova, A. I., and Solodkin, Ye. Ye., "Influence of Entropy Layer Absorption on Characteristics of Long Blunt Bodies Under Different Flow Conditions in the Boundary Layer" (in Russian), *Trudy TsAGI,* Issue 2107, pp. 161–200.

[15]Wang, K. S., "Separation Patterns of Boundary Layer over an Inclined Body of Revolution," *AIAA Journal,* Vol. 10, No. 8, 1972, pp. 1044–1050.

[16]Werle, H., "Separation on Axisymmetrical Bodies at Low Speeds," Recherche Aeronautique, No. 90, 1962, pp. 3–14.

[17]Miller, Ch. G., Gnoffo, P. A., and Wilder, S. E., "Measured and Predicted Heating Distribution for Biconic at Mach 10," *Journal of Spacecraft and Rockets,* Vol. 23, No. 3, 1986, pp. 251–258.

[18]Ginoux, I. I., *Experimental Evidence of Three-Dimensional Perturbations in the Reattachment of Two-Dimensional Laminar Boundary Layer at M* = 2.05, von Karman Inst. for Fluid Dynamics, Belgium, 1958.

[19]Brazhko, V. N., "Periodic Flow Structure and Heat Transfer in the Supersonic Flow Attachment Region" (in Russian), *Uchenye Zapiski TsAGI,* Vol. 10, No. 2, 1979, pp. 113–118.

[20]Brazhko, V. N., "Experimental Investigation of Separated Flow Geometry and Heat Transfer Behind an Axisymmetric Step" (in Russian), *Trudy TsAGI,* Issue 1493, 1973, pp. 21–35.

[21]Roshko, A., and Thomke, G. I., "Observations of Turbulent Reattachment Behind an Axisymmetric Downstream-Facing Step in Supersonic Flow," *AIAA Journal,* Vol. 4, No. 6, 1966, pp. 975–980.

[22]Glotov, G. F., and Moroz, E. K., "Longitudinal Vortices in Supersonic Flows with Separation Zones" (in Russian), *Uchenye Zapiski TsAGI,* Vol. 8, No. 4, 1977, pp. 44–53.

[23]Khonichev, V. I., Mezentsev, A. V., and Yermolayev, I. K.,

"Heat Transfer in Attachment Zone of Turbulent Boundary Layer with Longitudinal Vortex Structures" (in Russian), Proceedings of the Heat/Mass Transfer Forum, Minsk, Belarus, Sec. 1, Pt. 1, May 24–27, 1988, pp. 113–115.

[24]Brazhko, V. N., and Shkirin, N. N., "Heat Transfer on Cones with an Isentropic Compression Surface" (in Russian), *Uchenye Zapiski TsAGI,* Vol. 17, No. 2, 1986, pp. 106–111.

[25]Borovoy, V. Ya., Kubyshina, T. V., Osipov, V. V., Ryzhkova, M. V., and Struminskaya, I. V., "Investigation of Heat Transfer on a Blunt Leading Edge of a Variable Sweep Wing in the Region of the Bow Shock Impingement" (in Russian), *Trudy TsAGI,* Issue 2107, 1981, pp. 127–145.

[26]Brazhko, V. N., "Experimental Investigation of Gas Flow and Heat Transfer in the Region of Slender Delta Semiwing-Plate Interference," (in Russian), *Trudy TsAGI,* Issue 2107, 1981, pp 32–42.

[27]Teterin, M. P., "Investigation of Gas Flow and Heat Transfer in the Region of Shock Impingement on a Cylinder in a High Supersonic Velocity Flow" (in Russian), *Izvestiya AN SSSR, Mekhanica Zhidkosti i Gaza,* No. 2, 1967, pp. 143–147, No. 3, 1967, pp. 92–97.

[28]Avduyevsky, V. S., and Medvedev, K. I., "Physical Flow Features in Three-Dimensional Separation Zones" (in Russian), *Heat/Mass Transfer*, Vol. 1, Energia, Moscow, 1968, pp. 140–147.

[29]Edney, B. E., "Effects of Shock Impingement on the Heat Transfer Around Blunt Bodies," *AIAA Journal,* Vol. 5, No. 1, 1968, pp. 15–21.

[30]Hains, F. D., and Keyes, I. W., "Shock Interference Heating in Hypersonic Flows," *AIAA Journal,* Vol. 10, No. 11, 1972, pp. 1441–1447.

[31]Borovoy, V. Ya., and Struminskaya, I. V., "Heat Transfer on a Cylinder in the Region of Plane Shock Impingement" (in Russian), *Trudy TsAGI,* Issue 2514, 1991, pp. 171–186.

[32]Zemlyansky, B. A., Lesin, A. B., Lunev, V. V., and Shmanenkova, G. A., "On Interference of Oblique Shock Waves of One Family in a Hypersonic Flow" (in Russian), *Izvestiya AN SSSR, Mekhanika Zhidkosti i Gaza,* No. 5, 1982, pp. 134–138.

[33]Avduyevsky, V. S., Danilov, Yu. I., Koshkin, V. K., Kutyrin, I. N., Mikhaylova, M. M., Mikheev, Yu. S., and Sergel, O. S., "Heat Transfer Fundamentals in Aeronautical and Rocket and Space Technology" (in Russian), Mashinostroyeniye, Moscow, 1975, pp. 320–324.

[34]Lamb, I. P., "Analysis and Correlation of Convective Heat Transfer Measurement for Open Cavities in Supersonic Flow," AIAA 15th Thermophysics Conf., AIAA Paper 80-0080, Snowmass, CO, July 14–16, 1980.

A Best-Selling Trilogy ✷ AIAA Education Series

AEROTHERMODYNAMICS OF AIRCRAFT ENGINE COMPONENTS

Gordon C. Oates, editor

Major topics include turbine cooling, boundary layer analysis in rotating machinery, engine noise, combustion, and afterburners.

1985, 551 pp, illus, Hardback
ISBN 0-915928-97-3
AIAA Members $46.95
Nonmembers $57.95
Order #: 97-3 (830)

AIRCRAFT PROPULSION SYSTEMS TECHNOLOGY AND DESIGN

Gordon C. Oates, editor

"....a practical reference text....excellent survey of important matters useful in aircraft design." —I. S. Gartshore, University of British Columbia

A comprehensive coverage of the key physical concepts that govern gas turbine propulsion systems. Topics include combustion technology, engine/airplane performance matching, inlets and inlet/engine integration, variable convergent/divergent nozzle aerodynamics, and more.

1989, 528 pp, illus, Hardback
ISBN 0-930403-24-X
AIAA Members $46.95
Nonmembers $57.95
Order #: 24-X (830)

AEROTHERMODYNAMICS OF GAS TURBINE AND ROCKET PROPULSION: REVISED AND ENLARGED

Gordon C. Oates

Contents include: thermodynamics and quasi-one-dimensional fluid flows; chemical and nonchemical rockets; ideal and nonideal cycle analysis; component performance; engine off-design performance; blade aerodynamics; SAE Gas Turbine Engine Notation appendices; and more.

1988, 452 pp, illus, Hardback
ISBN 0-930403-34-7
AIAA Members $46.95
Nonmembers $57.95
Order #: 34-7 (830)

Place your order today! Call 1-800/682-AIAA

AIAA

American Institute of Aeronautics and Astronautics
Publications Customer Service, 9 Jay Gould Ct., P.O. Box 753, Waldorf, MD 20604
Phone 301/645-5643, Dept. 415, FAX 301/843-0159

Sales Tax: CA residents, 8.25%; DC, 6%. For shipping and handling add $4.75 for 1-4 books (call for rates for higher quantities). Orders under $50.00 must be prepaid. Please allow 4 weeks for delivery. Prices are subject to change without notice. Returns will be accepted within 15 days.